Riesz-Laplace Wavelet Transform and PCNN Based Image Fusion

Shuifa Sun[1,2], Yongheng Tang[2,3], Zhoujunshen Mei[2], Min Yang[2],
Tinglong Tang[1,2], Yirong Wu[4]

[1]*Hubei Key Laboratory of Intelligent Vision Based Monitoring for Hydroelectric Engineering, China Three Gorges University, YiChang, China*

[2]*College of Computer and Information Technology, China Three Gorges University, YiChang, China*

[3]*College of Economics and Management, China Three Gorges University, YiChang, China*

[4]*Institute of Advanced Studies in Humanities and Social Sciences, Beijing Normal University, Zhuhai, China*

Corresponding author: Yirong Wu, yrwu@bnu.edu.cn

Abstract. Important information perceived by human vision comes from the low-level features of the image, which can be extracted by the Riesz transform. In this study, we propose a Riesz transform based approach to image fusion. The image to be fused is first decomposed using the Riesz transform. Then the image sequence obtained in the Riesz transform domain is subjected to the Laplacian wavelet transform based on the fractional Laplacian operators and the multi-harmonic splines. After Laplacian wavelet transform, the image representations have directional and multi-resolution characteristics. Finally, image fusion is performed, leveraging Riesz-Laplace wavelet analysis and the global coupling characteristics of pulse coupled neural network (PCNN). The proposed approach has been tested in several application scenarios, such as multi-focus imaging, medical imaging, remote sensing full-color imaging, and multi-spectral imaging. Compared with conventional methods, the proposed approach demonstrates superior performance on visual effects, contrast, clarity, and the overall efficiency.

Key words: image fusion, Riesz transform, polyharmonic spline, Laplacian wavelet, pulse coupled neural network, PCNN.

1. Introduction

Image fusion aims to integrate images obtained by different focusing positions or different kinds of sensors into one new image containing better description of the scene. Different focusing positions result in different sharpness for different areas of an image. In order to obtain clear images and more information, image fusion methods are usually adopted to solve this kind of multi-focus problem [9]. In addition to multi-focus problem, there are many other image fusion problems. With the development of new technology, there are more and more types of imaging sensors. Different sensors have different capabilities of acquiring different information. For example, for multi-band remote sensing images, full-color images and multi-spectral images can be collected by remote sensing satellite imaging equipment, in which full-color images have structure information with high spatial resolution, and multi-spectral images contain color information. Fused

images of these two kinds of images can be used to better describe actual ground information [21, 22]. At present, image fusion can be performed in either spatial domain or transform domain. Image fusion in spatial domain directly operates on the gray value of an image. This method cannot extract edge information, which results in low contrast for fusion results. Image fusion in transform domain attracts a lot of attention currently, including pyramid decomposition, wavelet transform and other multi-scale transforms. The pyramid-based image fusion method can retain the edge details of the original image and make the fusion image stable and anti-noise. But in the multi-scale structures of pyramid decomposition, the details of different resolutions are strongly correlated, so the fusion results are not satisfactory [18]. Wavelet transform is the most commonly used method in transform domain since it reduces the correlation between sub-band coefficients in terms of time-frequency local characteristics [2]. Leveraging these two methods, we develop an image fusion approach. In image fusion applications for either different focusing positions or different kinds of sensors, our proposed approach demonstrates superior performance on visual effects, contrast, clarity, and the overall efficiency.

2. Related works

Image can be fused at pixel-level, feature-level, or decision making-level. Most of studies focus on pixel-level and feature-level fusion [4, 17]. This structure information are often extracted in the transform domain instead of the spatial domain for image fusion since it is easier to separate this information by directly operating image gray values in the transform domain to obtain clearer and higher contrast images. Most of related studies in the transform domain focus on multi-resolution transform, such as pyramid decomposition, wavelet transform, super-wavelet transform, etc. [2, 18, 22]. Compared with pyramid-based decomposition, wavelet decomposition performs well in local frequency analysis, and reduces the correlation between sub-band coefficients [14]. The contourlet transform, one of the super-wavelets, has multi-directionality feature and can represent singular lines and surfaces in natural scenes better than wavelet transform [8]. Additionally, non-subsampled Contourlet Transform (NSCT) uses a sub-band separation method to avoid spectrum aliasing caused by up-down sampling process [21] but space and time complexity are increased. The common goal of this series of improvements is to better decompose images and gather related features to facilitate separation. In order to solve this problem, in this paper a fusion method of Riesz transform is proposed for unfused image, which can express the local structure information of an image well and maintain the consistency of low-level feature space [22]. Riesz transform has been widely used in computer vision and image processing, such as image quality evaluation based on image structure similarity after this transform [3, 10]. Because Riesz transform is isotropic and relatively easy to calculate, it is more efficient for detecting the edges of an image based on phase consistency in Riesz transform space than that in Hilbert transform space [11].

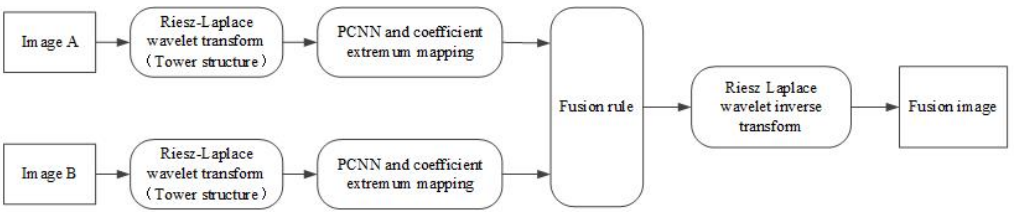

Fig. 1. Riesz-Laplace wavelet pyramid combined with PCNN image fusion process block diagram.

In this study, we propose a Riesz transform based image fusion approach by leveraging important characteristics of this transform, such as low-level feature preservation, locality and directionality. An image is first transformed into Riesz transform space. After this operation, the transformed images are further transformed into Laplacian wavelet transform space, so that the image has multi-resolution characteristics. The Laplacian wavelet transform not only reduces a large amount of redundant information in a single pyramid transform, but also has good spatial and frequency domain locality in the transform space, which can be used to well retain high-frequency information of the fused image [18]. Then, the unfused images of each layer are input into Pulse Coupled Neural Network (PCNN). PCNN is an improvement of the neuron model proposed by Eckhorn et al., which is based on the phenomenon of cerebral cortex sync pulse distribution in cats [12, 13]. It has the characteristics such as spatio-temporal summation, dynamic pulse release, vibration, and fluctuation caused by synchronous pulse release. It has been widely used in image denoising, enhancement, segmentation, edge detection, and fusion. In this paper, the multi-resolution image is processed by PCNN, and the neurons ignition frequency graph describing feature clustering is obtained. Then, based on the size of the ignition frequency graph, each scale of the original image is fused [13]. Finally, the results from PCNN are inversely transformed into the Riesz transform domain by Laplacian pyramid. The inverse transform of Riesz (here multiplied by the conjugate coefficient of Riesz transform) finally produces the fused image.

3. Riesz transformation principle

Since Gabor proposed analytic signal in 1946, Hilbert transform has been widely used in one-dimensional signal analysis. One-dimensional analytic signal is a complex signal composed of two parts. The first part is the real part, the original signal, and the second part is the imaginary part derived from Hilbert transform of original signal. Local amplitude and phase can be obtained based on one-dimensional analytic signal analysis. Before Riesz transform was developed, there have been many studies on two-dimensional extension of Hilbert transform. However, analytic signals obtained in these studies have the problem of information loss [11].

Riesz transform can be regarded as an extended Hilbert transform of one-dimensional signal in multi-dimensional space. It has similar properties to those of Hilbert transform. The representation of Hilbert transform kernel in frequency domain is as follows:

$$H(w) = -j \cdot \text{sign}(w) = -j\frac{w}{||w||}, \tag{1}$$

where w is the frequency of an one-dimensional signal. The transform kernel of the Riesz transform in frequency domain is a two-dimensional vector (R_x, R_y) containing two parts:

$$(R_x, R_y) = \left(\frac{w_x}{||w||}, \frac{w_y}{||w||}\right), \tag{2}$$

where w stands for for the two-dimensional vector $w = (w_x, w_y)$, $||w||$ is the modulo value of the vector $|w| = (w_x^2 + w_y^2)^{\frac{1}{2}}$.

When an image is defined as $f(x, y)$, any point on the image is defined as $P = (x, y)$, the Riesz transform kernel in space domain can be described by

$$(r_x, r_y) = \left(\frac{x}{2\pi\,||p||^3}, \frac{y}{2\pi\,||p||^3}\right). \tag{3}$$

Riesz transform of an image can be expressed by equation (4), where $*$ represents a convolution operation. The image in spatial domain is convolved with two Riesz transform kernels separately.

$$f_r(P) = \begin{pmatrix} f_{r_x} \\ f_{r_y} \end{pmatrix} = \begin{pmatrix} f(P) * r_x \\ f(P) * r_y \end{pmatrix}. \tag{4}$$

In the frequency domain, the image is first transformed by Fourier transform. Then, it is multiplied by the frequency domain Riesz transform kernel:

$$F_R(w) = \begin{pmatrix} F_{R_x} \\ F_{R_y} \end{pmatrix} = \begin{pmatrix} R_x \cdot F(w) \\ R_y \cdot F(w) \end{pmatrix}. \tag{5}$$

The second-order transform of the Riesz transform is expressed as follows:

$$\begin{cases} R_{xx}[f](P) = R_x[R_x[f](P)](P) \\ R_{xy}[f](P) = R_y[R_x[f](P)](P) \\ R_{yy}[f](P) = R_y[R_y[f](P)](P) \end{cases}. \tag{6}$$

The first-order feature map can well express the edge contour features of the image, and the second-order feature map can express more complex features, such as corner points. As shown in Fig. 2, R_x and R_{xx} highlight the horizontal contour of the image, R_y and R_{yy} the vertical contour, and R_{xy} the diagonal profile [14,17]. The higher-order Riesz transform is directional [8].

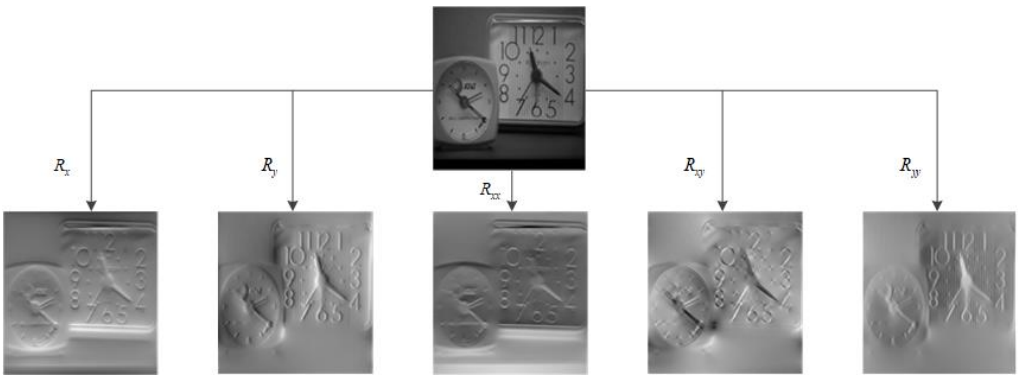

Fig. 2. First and second order Riesz transform image schematic diagram, the first row of images (source images) comes from the TestingImageDataset in the image fusion standard database [16], and the second row of images is the first-order feature map and second-order feature map after Riesz transformation.

4. Laplacian wavelet transform based on Riesz transform

Based on the Riesz transform, Laplacian spline wavelets are used for multiresolution decomposition. The fractional Laplacian operator $(-\Delta)^{\alpha}$, $\alpha \in R^{+}$, is an isotropic differential operator of order 2α. In Fourier domain it is defined as:

$$(-\Delta)^{\alpha} f(x) \xrightarrow{\text{FT}} ||w||^{2\alpha} \hat{f}(w)\,. \tag{7}$$

The multi-harmonic spline is a spline function related to the fractional Laplacian operator, and the γ-order multi-spline function $\varphi_{\gamma}(x)$ satisfies:

$$s(x) = \sum_{k \in Z^2} s[x] \varphi_{\gamma}(x-k)\,, \tag{8}$$

where $s[x] = s(x)|_{x=k}$ is the integer sample of $s(x)$ at k. The Fourier response of $\varphi_{\gamma}(x)$ is described as:

$$\varphi_{\gamma}(x) \xrightarrow{FT} \hat{\varphi}_{\gamma}(w) = \frac{||w||^{-\gamma}}{\sum_{k \in Z^2} ||w+2\pi k||^{-\gamma}}\,. \tag{9}$$

With the above concepts of fractional differential operators and multi-harmonic splines, a symmetric fractional order ($\gamma > \frac{1}{2}$) Laplacian spline wavelet can be defined as:

$$\psi(x) = (-\Delta)^{\frac{\gamma}{2}} \varphi_{2\gamma}(Dx)\,, \tag{10}$$

where $\varphi_{2\gamma}$ is the 2γ order multi-harmonic spline interpolation operator; the parameter of D is the down-sampling matrix. The basis function defined by $\psi(x)$ is:

$$\psi_{i,k}(x) = |det(D)|^{\frac{i}{2}}\, \psi(D^i x - D^{-1}k)\,, \tag{11}$$

where the parameters i, k are the scaling and translation coefficients, respectively. The Riesz transform is performed on the Laplacian wavelet base to obtain complex Riesz Laplacian wavelets of order $\gamma(\gamma > \frac{1}{2})$:

$$\psi'(x) = R\psi(x) = R(-\Delta)^{\frac{\gamma}{2}} \varphi_{2\gamma}(Dx)\,. \tag{12}$$

5. The fusion process

We observe that low-level features of an image are separated well by Riesz Laplacian wavelet transform. Additionally, the selection of proper fusion rules is also important in the whole process of image fusion. This paper uses the Pulse Coupled Neural Network to perform image fusion at each layer of the Riesz-Laplace wavelet transform pyramid.

Pulse Coupled Neural Network is a bionic model proposed by Eckhorn in the 1990s, and is based on synchronous pulses in the cerebral cortex of animals such as cats and monkeys. PCNN is a simplified neural network which imitates the principle of cat vision. It is a feedback network composed of several interconnected neurons and has the effect of synchronous pulse release [12, 13].

The traditional PCNN fusion rules are:

$$I^k_{F.l}(x,y) = \begin{cases} I^k_{A.l}(x,y) & T^k_{A.l}(x,y) \geq T^k_{B.l}(x,y) \\ I^k_{B.l}(x,y) & T^k_{A.l}(x,y) < T^k_{B.l}(x,y) \end{cases}, \tag{13}$$

where $I^k_{A.l}(x,y)$ and $I^k_{B.l}(x,y)$ are the wavelet coefficients of the source image A and the source image B, and $T^k_{A.l}(x,y)$ and $T^k_{B.l}(x,y)$ are the numbers of firings corresponding to the wavelet coefficients.

The steps of PCNN image fusion based on Riesz-Laplace wavelet transform are described as follows:

a) Riesz-Laplace wavelet transform is applied to the unfused image A and B to obtain the pyramid structures of the images. Laplacian wavelet transform based on Riesz transform has the coefficients of each layer are $I^k_{A.l}(x,y,i)$ and $I^k_{B.l}(x,y,i)$.
b) The wavelet coefficients of each layer obtained from a) are input into the PCNN network separately, and iterate $N_{\max}$ times to obtain the respective ignition maps of each layer, called also signature maps, denoted as $\mathrm{MF}_{A.i}$ and $\mathrm{MF}_{B.i}$.
c) The pixel points with a larger ignition time at each layer are taken as the fusion coefficients for image fusion.
d) The inverse Riesz Laplacian wavelet transform is finally performed on obtained coefficients to recover the fused image.

6. Experiment and result analysis

6.1. Experimental description

The quality of fused images can be evaluated subjectively and objectively. In order to objectively test the method of this paper, to verify the universality and accuracy of the algorithm in this paper, in this experiment multiple images in different scenes from the image fusion standard database for fusion testing are randomly selected, and compared with LP-PCNN [5] (its preliminary version can be found in [6]) and NCST-PCNN [23] algorithms. Among them, the selected image data comes from TestingImageDataset from [15] (mainly including multi-focus image fusion data), Harvard [7] (mainly including medical image fusion data), and three Gaofen data bases: GF-1, GF-2 and GF-3 from [1] (mainly including remote sensing image fusion data) in the image fusion standard database [16].

The experimental environment of this article is 11th Gen Intel(R) Core (TM) i7-11700 @ 2.50 GHz, memory 16 GB, 64-bit Win10 operating system, and Matlab R2018b programming environment [20] in which multi-spectral and full-color remote sensing images have multiple bands. For this kind of images, first, they are converted from RGB space to HIS space. The I component (I represents the I component of HIS image) containing the main structure information is fused with full-color remote sensing image using the method proposed in this paper. Then the new I component and the multispectral H and S components with spectral features are transformed back to the RGB space. The images to be fused in this paper have been initially registered. The results of image fusion are shown in Fig. 3.

6.2. Subjective evaluation

Subjective evaluation mainly depends on human visual effects. Three methods including Laplacian pyramid decomposition and restoration(, LP-PCNN [5] (also [6]), NCST-PCNN [23] and our method have been used to fuse three different types of images. For multi-focusing clock image, the decomposition of the Laplacian pyramid produces artifacts. NSCT-PCNN and our method perform well. For medical images, Laplacian decomposition produces artifacts, which is not good for medical diagnosis. The fusion effects of NSCT-PCNN and our method are similar. For remote sensing images, images fused by the Laplacian pyramid method are dark. The fusion effects of NSCT-PCNN and our method are superior to LP-PCNN.

In particular in Fig. 3, the images in the first row are the two images to be fused, and the images in the second row represent images generated by fusion of three different methods, where (1) represents Laplacian Pyramid decomposition and restoration using Pulse Coupled Neural Network fusion strategy (LP-PCNN) method. The result map generated by fusion (2) represents the result map generated by the fusion of non-downsampled

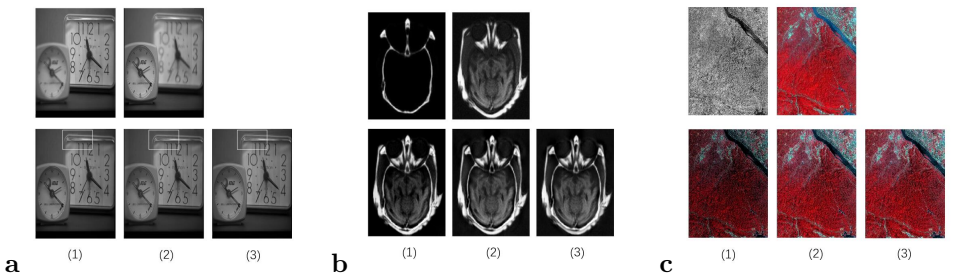

Fig. 3. Image fusion results. (**a**) The Clock fusion; (**b**) Medical CT, MRI fusion; (**c**) Remote sensing full-color and multi-spectral image fusion. Laplacian Pyramid decomposition and restoration using Pulse Coupled Neural Network fusion strategy (LP-PCNN) (1), non-downsampled contourlet transform decomposition and restoration (NSCT-PCNN) (2), and Riesz fractional Laplacian Pyramid decomposition and restoration (*Ours*) (3) fusion methods test for the above multi-scenario application. The white window is to focus on the details to illustrate the comparative advantages of the fusion results of this method and the fusion results of other methods. Taking the multi-focus clock image as an example in Fig. 3(a), the method of LP-PCNN will produce artifacts, while NSCT-PCNN and the method proposed in this paper perform well.

contourlet transform decomposition and restoration ($NCST\_PCNN$) method, and (3) represents the result map generated by the fusion method of this paper.

6.3. Objective evaluation

In order to evaluate the fusion results more comprehensively, objective indexes are used in this paper. Objective evaluation of the effect of image fusion is standard and deterministic. For this reason, in this paper the information entropy (IE), standard deviation (SD), and average gradient (AG) defined in the literature [19] were chosen to evaluate the fusion results objectively. This kind of evaluation index is to use the fused image itself or some feature statistics to measure the quality of the fused image, and then make an objective evaluation of the performance of the image fusion technology. The specific meanings of each evaluation index are as follows. 1. Information entropy is an important index to measure the information richness of an image. The larger the entropy value, the more information the image contains. 2. The larger the standard deviation, the more dispersed the gray level distribution of the image, the greater the contrast, and more information can be seen, the better the image quality; the smaller the standard deviation, the worse the image quality. The smaller the contrast of the image, the image is closer to an image with single and uniform tone, and not much information can be seen. 3. The average gradient can sensitively reflect the clarity of the image, and the larger the average gradient, the richer the information obtained from the source image of the fused image, and the better the fusion.

Information Entropy (IE)
Information entropy reflects the richness of image information.

$$\mathrm{IE} = -\sum_{i=0}^{L-1} P_i \ln P_i \,. \tag{14}$$

In the formula, P_i represents the ratio of the number of pixels with gray value i in the image to the total number of pixels in the image, which reflects the probability distribution of pixels with gray value i in the image. The larger the value of IE, the richer the information and the better the quality of the fused image.

Standard Deviation (SD)
The standard deviation indicates the degree of dispersion of the data. The larger the standard deviation, the more discrete the data, and the larger the standard deviation, the larger the contrast is reflected in the image.

$$\mathrm{SD} = \sqrt{\frac{1}{X \times Y} \sum_{x=1}^{X} \sum_{y=1}^{Y} (p(x,y) - \mu)^2} \,. \tag{15}$$

In the formula, μ represents the mean value of the gray value of the image, which reflects the average brightness of the image, and the standard deviation reflects the sharpness and contrast of the image. The higher the SD value, the better the contrast and the clearer the fusion result.

Average Gradient (AG)
Average Gradient (AG) reflect the clarity of the image, The larger the AG value, the clearer the fused image and the better the quality.

$$\begin{cases} AG_v = \frac{\sum_{x=0}^{X-1} \sum_{y=0}^{Y-2} |p(x+1,y) - p(x,y)|}{(X-1) \times Y} \\ AG_h = \frac{\sum_{x=0}^{X-2} \sum_{y=0}^{Y-2} |p(x,y+1) - p(x,y)|}{X \times (Y-1)} \end{cases} \quad AG = \sqrt{{AG_v}^2 + {AG_h}^2} \,. \tag{16}$$

In practical applications, time complexity is an important factor in decision making for algorithm selection. In this study, the efficiency of algorithms is also one of the criteria to evaluate the quality of algorithms. The statistical results are described in Table 1, in which the multi-spectral and full-color image results are the mean of three-channel results. The values of IE, SD, and AG are positively correlated with the fusion effects; the higher the values, the better image fusion effects. In multi-focus image fusion and CT/MRI image fusion, our method performs better than NSCT-PCNN method, especially in time complexity analysis. Compared with the Laplacian decomposition method, our method produces higher IE values, the image results are shown in Fig. 3(a) and Fig. 3(b). In multi-spectral and full-color image fusion, our method produces higher index values than other algorithms, the image results are shown in Fig. 3(c).

Tab. 1. Image fusion evaluation statistics.

Unfused Images	Fusion method	IE	SD	AG	Time [s]
Multi-focus	LP-PCNN [5]	7.060268	0.016244	42.227196	1.6965
	NSCT-PCNN [23]	7.040197	0.015665	40.550226	216.167
	Ours	7.104631	0.016058	41.508493	6.754
CT/MRI	LP-PCNN [5]	5.690078	0.082494	63.087874	0.331
	NSCT-PCNN [23]	6.838788	0.077755	58.903765	46.815
	Ours	6.969029	0.080016	60.576231	1.425
multi-spectral and full-color	LP-PCNN [5]	6.479447	0.209883	35.579854	34.625
	NSCT-PCNN [23]	7.227013	0.232942	46.672342	4710.249
	Ours	7.227010	0.232942	46.672549	116.220

7. Conclusion

In this study, we propose a Riesz transform based approach to image fusion. Specifically, an image is decomposed by Riesz Laplacian spline wavelet pyramid to derive a new representation, with which PCNN optimization is employed to obtain fused images. Through subjective observation and objective index analysis, we observe that our method demonstrates superior performance in image fusion with low time complexity. Through experiments, we find that our method can be further optimized by selecting PCNN parameters adaptively. Another future work is to choose Riesz transform as the objective function of fusion rules to improve fusion effects further.

Acknowledgement

This work is supported by the National Natural Science Foundation of China (NSFC) under contract No. 61871258.

References

[1] European Space Agency and H. Kramer. Satellite Missions catalogue. `https://directory.eoportal.org/web/eoportal/satellite-missions`.

[2] S. Bhat and D. Koundal. Multi-focus image fusion using neutrosophic based wavelet transform. *Applied Soft Computing*, 106:107307, 2021. doi:10.1016/j.asoc.2021.107307.

[3] T. A. Bui and X. T. Duong. Higher-order Riesz transforms of Hermite operators on new Besov and Triebel–Lizorkin spaces. *Constructive Approximation*, 53:85–120, 2021. doi:10.1007/s00365-019-09493-y.

[4] J. Chen, L. Chen, and M. Shabaz. Image fusion algorithm at pixel level based on edge detection. *Journal of Healthcare Engineering*, page 5760660, 2021. doi:10.1155/2021/5760660.

[5] K. J. He, X. Jin, R. Nie, D. M. Zhou, Wang Q., and Yu J. Color image fusion based on simplified PCNN and Laplace pyramid decomposition (in Chinese). *Journal of Computer Applications*, 2016(S1):133–137, 2016.

[6] X. Jin, R. Nie, and D. M. Zhou. Color image fusion researching based on S-PCNN and Laplacinan pyramid. In *Proc. 2nd Int. Conf. Cloud Computing and Big Data in Asia CloudCom-Asia 2015*, volume 9106 of *Lecture Notes in Computer Science*, pages 179–188, Huangshan, China, 17-19 Jun 2015. doi:10.1007/978-3-319-28430-9_14.

[7] K. A. Johnson and J. A. Becker. The whole brain Atlas. `https://www.med.harvard.edu/AANLIB/`. Harvard Medical School.

[8] W. Li, Q. Liu, K. Wang, and K. Cai. Improving medical image fusion method using fuzzy entropy and nonsubsampling contourlet transform. *International Journal of Imaging Systems and Technology*, 31(1):204–214, 2021. doi:10.1002/ima.22476.

[9] Y. Liu, L. Wang, J. Cheng, C. Li, and X. Chen. Multi-focus image fusion: A survey of the state of the art. *Information Fusion*, 64:71–91, 2020. doi:10.1016/j.inffus.2020.06.013.

[10] Y. F. Lu and T. Zhang. Image quality assessment method via Riesz-transform based structural similarity. *Chinese Journal of Liquid Crystals and Displays*, 30(6):992–999, 2015. doi:10.3788/YJYXS20153006.0992.

[11] S. Moritoh and N. Takemoto. Expressing Hilbert and Riesz transforms in terms of wavelet transforms. *Integral Transforms and Special Functions*, 34(5):365–370, 2023. doi:10.1080/10652469.2022.2126465.

[12] C. Panigrahy, A. Seal, and N. K. Mahato. MRI and SPECT image fusion using a weighted parameter adaptive dual channel PCNN. *IEEE Signal Processing Letters*, 27:690–694, 2020. doi:10.1109/LSP.2020.2989054.

[13] C. Panigrahy, A. Seal, and N. K. Mahato. Parameter adaptive unit-linking dual-channel PCNN based infrared and visible image fusion. *Neurocomputing*, 514:21–38, 2022. doi:10.1016/j.neucom.2022.09.157.

[14] A. I. Rahmani, M. Almasi, N. Saleh, and M. Katouli. Image fusion of noisy images based on simultaneous empirical wavelet transform. *Traitement du Signal*, 37(5):703–710, 2020. doi:10.18280/ts.370502.

[15] S. Savić. Multifocus Image Fusion. `https://dsp.etfbl.net/mif/`. Chair of General Electrical Engineering, Faculty of Electrical Engineering, University of Banja Luka, Republic of Srpska.

[16] S. Savić and Z. Babić. Multifocus image fusion based on the first level of empirical mode decomposition. In *Proc. 19th Int. Conf. Systems, Signals and Image Processing IWSSIP 2012*, pages 604–607, Vienna, Austria, 11-13 Apr 2012. IEEE. `https://ieeexplore.ieee.org/abstract/document/6208315`.

[17] S. Singh, N. Mittal, and H. Singh. A feature level image fusion for IR and visible image using mNMRA based segmentation. *Neural Computing and Applications*, 34(10):8137–8145, 2022. doi:10.1007/s00521-022-06900-7.

[18] J. Sun, Q. Han, K. Liang, L. Zhang, and Z. Jin. Multi-focus image fusion algorithm based on Laplacian pyramids. *Journal of the Optical Society of America A*, 35(3):480–490, 2018. doi:10.1364/JOSAA.35.000480.

[19] L. F. Tang, H. Zhang, H. Xu, and J. Y. Ma. Deep learning-based image fusion: A survey. *Journal of Image and Graphics*, 28(1):3–36, 2023. doi:10.11834/jig.220422.

[20] The MathWorks, Inc. MATLAB. Natick, MA, USA. [Accessed: 2018]. `https://www.mathworks.com`.

[21] X. Tian, W. Zhang, Y. Chen, Z. Wang, and J. Ma. Hyperfusion: A computational approach for hyperspectral, multispectral, and panchromatic image fusion. *IEEE Transactions on Geoscience and Remote Sensing*, 60:5518216, 2021. doi:10.1109/TGRS.2021.3128279.

[22] Y. Xing, S. Yang, Z. Feng, and L. Jiao. Dual-collaborative fusion model for multispectral and panchromatic image fusion. *IEEE Transactions on Geoscience and Remote Sensing*, 60:5400215, 2020. doi:10.1109/TGRS.2020.3036625.

[23] J. J. Yang. Improved gradient image fusion algorithm based on NSCT and PCNN. *Digital Technology and Application*, (11):124–127, 2015. doi:10.19695/j.cnki.cn12-1369.2015.11.092.